Resolution of Patch Capacitance Recordings and of Fusion Pore Conductances in Small Vesicles

Knut Debus* and Manfred Lindau†

*Department of Molecular Cell Research, Max Planck Institute for Medical Research, D-69120 Heidelberg, Germany, and †School of Applied and Engineering Physics, Cornell University, Ithaca, New York 14853 USA

ABSTRACT We investigated the noise levels in cell-attached patch capacitance recordings with a lock-in amplifier. The capacitance noise level decreases with increasing sine wave frequency up to 20–40 kHz. With a 20-mV rms sine wave the rms noise level above 8 kHz is <50 aF. With increasing sine wave amplitudes a further reduction down to 14 aF could be achieved. Capacitance measurements with a lock-in amplifier may also be used to measure the conductance of fusion pores connecting the vesicular lumen to the extracellular space. It is estimated that at noise levels of 14 aF fusion pore conductances between 20 pS and 700 pS may be resolved in vesicles with 380-aF capacitance by using a 50-kHz sine wave. This corresponds to vesicles with a ~110-nm diameter. It is suggested that with low-noise techniques fusion pores may be detectable in vesicles approaching the size of large synaptic vesicles.

INTRODUCTION

Single exocytotic events can be characterized by time-resolved patch-clamp capacitance measurements with a lock-in amplifier (for a review see Lindau, 1991). Exocytosis of individual vesicles has been resolved as stepwise increases in membrane capacitance (Neher and Marty, 1982; Fernandez et al., 1984). Capacitance measurements revealed that fusion may in some cases be transient, as indicated by transient capacitance changes, also called capacitance flickers, indicating that several steps in exocytotic fusion are reversible (Neher and Marty, 1982; Fernandez et al., 1984). It has thus been possible to determine the rates of opening and closing of fusion pores from capacitance measurements (Oberhauser et al., 1992; Oberhauser and Fernandez, 1996), similar to determination of the rates at which ion channels open and close from single-channel recordings. In addition to a characterization of the kinetic properties, the electrical conductance of fusion pores has also been determined. One method uses the analysis of a current transient that occurs upon fusion of a vesicle with the plasma membrane. This current transient charges the membrane of the vesicle to the holding potential applied to the plasma membrane immediately after fusion pore formation (Breckenridge and Almers, 1987; Spruce et al., 1990; Hartmann and Lindau, 1995). With this method the fusion pore conductance can be measured during the first millisecond of its existence (Breckenridge and Almers, 1987; Spruce et al., 1990; Hartmann and Lindau, 1995). Another method uses the analysis of the lock-in amplifier signals to determine the fusion pore conductance (Alvarez de Toledo and Fernandez, 1987; Breckenridge and Almers, 1987; Spruce et al., 1990; Lindau, 1991; Alvarez de Toledo et al., 1993; Curran et al., 1993; Lindau et al., 1993; Hartmann and Lindau, 1995; Lollike et al., 1995; Albillos et al., 1997; Ratinov et al., 1998). This second method has a lower time resolution but allows us to monitor fusion pore conductances over long time periods. These methods thus made it possible to characterize the conductance and dynamics of single fusion pores similar to those of single ion channels, and it may be expected that single fusion pore recordings will be essential to the characterization of the molecular identity of fusion pores, just as single-channel recordings were instrumental in the identification of ion channel proteins.

Most of the fusion pore studies were performed using the whole-cell patch-clamp technique on cells with very large granules like mast cells or eosinophils, because the unavoidable noise of the RC circuit formed by access resistance and membrane capacitance (Neher and Marty, 1982; Lindau and Neher, 1988; Gillis, 1995) requires large granules to obtain detectable signals. Unfortunately, little is known about the molecules involved in exocytosis in these cell types. In the last few years it has been demonstrated that proteins of the SNARE complex (Söllner et al., 1993) play an important role in exocytosis in neurons and neuroendocrine cells (for a review see Morgan and Burgoyne, 1997). However, the vesicles involved in neurosecretion have diameters in the range of 30–300 nm, corresponding to a granule membrane capacitance of only 0.03–3 fF, and very little is known about single fusion events. In bovine chromaffin cells only exocytosis of a few exceptionally large vesicles could be resolved as capacitance steps in the whole-cell patch-clamp configuration (Robinson et al., 1995).

Current recordings from small membrane patches show considerably lower noise levels than whole-cell measurements (Hamill et al., 1981) because of the much smaller capacitance of the patch. Accordingly, capacitance measurements with significantly higher resolution can be made in the cell-attached configuration (Neher and Marty, 1982;

Received for publication 2 August 1999 and in final form 22 February 2000.

Address reprint requests to Dr. Manfred Lindau, School of Applied and Engineering Physics, Cornell University, 217 Clark Hall, Ithaca, NY 14853-2501. Tel.: 607-255-5264; Fax: 607-255-7653; E-mail: ml95@cornell.edu.

0006-3495/00/06/2983/15 $2.00

Lollike et al., 1995; Albillos et al., 1997). With this method capacitance noise levels as low as 25 aF (rms) have been attained, and fusion pore conductances could be resolved in vesicles with a capacitance of 650 aF, corresponding to a vesicle diameter of 150 nm (Lollike et al., 1995).

We investigated the dependence of the signal-to-noise ratio (SNR) of patch capacitance measurements on sine wave frequency and amplitude. We demonstrate that noise levels of 15 aF may be routinely obtained. For larger synaptic vesicles (~100 nm diameter) with a capacitance of 300 aF, fusion pores with conductances between 6 and 120 pS could then be resolved.

MATERIALS AND METHODS

Cells

Neuroblastoma-glioma NG 108-15 cells (ECACC, Salisbury, UK) were cultured in Dulbecco's modified Eagle medium (DMEM) (GIBCO, Sigma, Bio Whittaker) supplemented with 10% fetal calf serum (Sigma), 2 mM glutamine (Sigma), 2% HAT (hypoxanthine, aminopterine, thymidine) media supplement (50×; GIBCO), and 1% penicillin/streptomycin (each 10,000 U/μg; PAA). For patch-clamp experiments, 3000–4000 cells were plated on 12-mm-diameter coverslips and covered with DMEM containing 1% fetal calf serum, 2 mM glutamine, 2% HT (hypoxanthine, thymidine) media supplement (50×; GIBCO), 18 mg/100 ml theophylline (Sigma), and 1 μM prostaglandin E1 (Sigma). Cells were used within 4 days after plating.

Pipettes and solutions

Patch pipettes were pulled from thin-walled borosilicate glass capillaries with an outer diameter of 1.8 mm and a wall thickness of 0.18 mm (Hilgenberg, Malsfeld, Germany), using a two-stage L/M-3P-A puller (List Medical, Darmstadt, Germany), and coated with sticky wax (Kerr, Emeryville, CA). The pipette length was ~3.5 cm. The same standard solution was used in the bath and pipette. Standard saline contained 140 mM NaCl, 5 mM KCl, 1 mM $MgCl_2$, 2 mM $CaCl_2$, 10 mM HEPES, and ~30 mM glucose. The pH was adjusted to ~7.2 using NaOH, and the osmolality was ~305 mmol/kg. Pipettes immersed in the bath had a typical resistance of 2.5 MΩ (range 1.6–4.4 MΩ). Seal resistances in the cell-attached configuration were >10 GΩ.

Experimental set-up

Recordings were made using an EPC-7 patch-clamp amplifier (List Medical) and a two-phase analog lock-in amplifier (model PAR 5210; Princeton Applied Research, Princeton, NJ). Capacitance measurements were carried out using 20-mV (rms) sine wave command voltages, unless otherwise stated. For all frequencies used, the lock-in output filter was set to a time constant RC = 10 ms and a 12-dB rolloff, lock-in input filter set to *bandpass* and dynamic reserve set to *norm*. If not stated otherwise, the EPC-7 was operated in the high-gain range, using the 50-GΩ feedback resistor. Usually the gain was 50 mV/pA, although higher gain settings were used in some measurements at low frequencies. The input sensitivity of the lock-in amplifier was set at 1 V, giving a 10-V output for a 1-V rms (i.e., for a ±1.4-V amplitude) synchronous sine wave at the input. Because the output range of the EPC-7 is ~10 V rms and to prevent saturation of the lock-in amplifier, the current monitor output was connected to the lock-in input via a 10 kΩ:100 kΩ voltage divider. When resistors in the MΩ range were used, the voltage divider in conjunction with the input capacitance of the lock-in amplifier formed an unacceptable low-pass filter attenuating high-frequency signals. The lock-in outputs where sampled by a 16-bit A/D converter connected to an Atari Mega STE computer. The pulse for sealing was generated by a Wavetek (model 29; Wavetek, San Diego, CA). In some noise measurements (see the Results) an EPC-9 amplifier (HEKA, Lambrecht, Germany) was used instead of the EPC-7. The EPC-9 was controlled by a second Atari Mega STE computer. Because the EPC-9 can provide a pulse for sealing, the pulse generator was omitted.

Phase adjustment and calibration of capacitance measurements

The EPC-7 was equipped with a capacitance dither switch adding a resistor in series with the C_{slow} potentiometer. The C_{slow} potentiometer was set to the smallest possible value, and the series conductance was set to 0.2 μS [1/(5 MΩ)]. With the sine wave voltage switched on, the current was nulled, using C_{fast} and τ_{fast}. The switch produced a defined capacitance compensation change of 200 fF, allowing for coarse phase adjustment and providing an approximate calibration step. For each recording the phase was readjusted and the calibration calculated as described later. To prevent saturation at high frequencies, the sine wave voltage had to be reduced by using the stimulus scaling switch while the dithering was done (Lollike et al., 1995). With the EPC-9 dithering of the C_{fast}, control software was used to change the compensation by 10–200 fF, depending on gain and lock-in frequency.

As in the whole-cell configuration, a change in the capacitance compensation produces an admittance change leading to a change in the sine wave current. Analogous to whole-cell capacitance measurements with the piecewise-linear technique (Neher and Marty, 1982; Lindau and Neher, 1988; Gillis, 1995), the phase of the lock-in should be set such that the capacitance calibration is reflected only in the Y2 output and not in the Y1 output of the lock-in amplifier. Assuming that the seal conductance is negligible, the phase setting for the lock-in is given by

$$\Phi = -2 \tan^{-1}(\omega\tau),$$

where $\omega = 2\pi f$ (f = sine wave frequency) and τ is the patch charging time constant. The change in rms current amplitude measured at the capacitance phase is

$$\Delta I_{pip} = V_0 |T(\omega)|^2 \omega \Delta C, \quad (1)$$

where V_0 is the rms sine wave voltage amplitude and

$$|T(\omega)|^2 = \frac{1}{1 + (\omega\tau)^2}.$$

The resulting change at the lock-in output V_{out} is

$$\Delta V_{out} = G t(f) \Delta I_{pip}, \quad (2)$$

where G is the gain of the patch-clamp amplifier (the voltage divider and the lock-in amplifier gain compensate each other), and $t(f)$ is the frequency-dependent transmission of the setup. This includes the frequency response of all instruments in the signal pathway. It is dominated by the patch-clamp amplifier and depends on the settings of the internal filters. $t(f)$ was measured by applying the sine wave from the lock-in to the headstage, using the "Test" mode of the patch-clamp amplifier, and reading the rms value of the output signal from the lock-in display. The lock-in was operating in the *r*, theta mode. $t(f)$ was determined separately for all different patch-clamp amplifier settings used here.

To determine the time constant τ_{slow} of the EPC-7 compensation network when set to the smallest possible capacitance value and a G_{series} value of 0.2 μS, the responses to C_{slow} dithering were measured at different frequencies between 800 Hz and 40 kHz. The changes ΔV_{out} were nor-

malized to dithering step size, gain, frequency response, and sine wave amplitude and plotted as a function of frequency. The relation

$$\frac{\Delta V_{out}}{\Delta C G t(f) V_0} = \omega |T(\omega)|^2 = \frac{2\pi f}{1 + (2\pi f\tau)^2}$$

was fitted, giving $\tau_{slow} = 1.9 \pm 0.1$ μs. The time constant τ_{patch} for charging the Ω-shaped patch via the access resistance of the pipette tip may, of course, be different, and the phase of the traces had to be rotated in the analysis by a few degrees ($\Delta\Phi$) such that capacitance changes occurring in the patch are confined to the *Y*2 trace. This phase shift can be calculated from the changes $\Delta Y1_C$ and $\Delta Y2_C$ produced by a pure capacitance change (see Results) as

$$\Delta\Phi = \tan^{-1}\left(\frac{\Delta Y1_C}{\Delta Y2_C}\right).$$

The correct phase of the patch Φ_{patch} is obtained by subtracting the phase shift $\Delta\Phi$ from the phase corresponding to τ_{slow} ($\Phi_{slow} = -2\tan^{-1}(\omega\tau_{slow})$):

$$\Phi_{patch} = -2\tan^{-1}(\omega\tau_{patch}) = -2\tan^{-1}(\omega\tau_{slow}) - \Delta\Phi.$$

The time constant τ_{patch} is then obtained as

$$\tau_{patch} = -\frac{1}{\omega}\tan\left(\frac{\Phi_{patch}}{2}\right).$$

The mean value for τ_{patch} in actual recordings was ~2.4 μs (see Results). For all measurements we thus used the following calibration formula:

$$\Delta C = \frac{\Delta V_{out}}{V_0 \omega |T(\omega)|^2 G t(f)}, \quad (3)$$

assuming $\tau = 2.4$ μs to calculate the calibration factor $|T(\omega)|^2$. With this value $|T(\omega)|^2$ is >0.9 up to ~20 kHz. Even for the slowest patch time constant observed in our measurements (4.5 μs), $|T(\omega)|^2$ is >0.9 up to 10 kHz. In these ranges the capacitance dithering thus provides a proper calibration value and recalibration using τ_{patch} is not necessary. Under these conditions determination of the frequency response *t*(*f*) is not required.

Determination of capacitance noise

To account for drifts or slow variations in the capacitance record, segments of capacitance traces were fitted by an appropriate polynomial, and the fitted line was subtracted from the measured data points. In cell-attached recordings segments were selected that contained no obvious capacitance steps or flickers. The rms deviations of the fit residuals gave the noise level of V_{out}, which was then converted into capacitance noise, using Eq. 3. The capacitance noise is inversely proportional to the signal-to-noise ratio (SNR) for a given capacitance step size.

This method eliminated linear drifts and low-frequency fluctuations in the range below 0.2 Hz. However, it does not have a well-defined frequency dependence, as could be obtained with a digital high-pass filter. On the other hand, digital high-pass filtering did not efficiently remove linear drifts and could not be applied to raw data, because stepwise capacitance changes also contain low-frequency components. Digital high-pass filters also showed marked oscillations in the pass band. The subtraction of slow changes by the use of polynomial fits of low order to selected recording segments was found to be most suitable for noise analysis of capacitance measurements. This method also closely resembles baseline subtraction methods used for precise step size determination and fusion pore analysis (Hartmann et al., 1995).

Noise bandwidth of the recording system

The theoretical equivalent noise bandwidth of a two-stage RC filter is $b_n = 1/(8RC)$. A lock-in amplifier acts like a bandpass centered at the reference frequency with an equivalent noise bandwidth Δf_{ENBW} that is twice that of the low-pass filter. For the settings used here (10 ms, 12 dB) this corresponds to 25 Hz. However, random noise is not a synchronous signal and should be equally distributed between the two output channels such that the effective gain is reduced by 3 dB per channel. Furthermore, Δf_{ENBW} is somewhat affected by internal settings of the lock-in input filter and the dynamical reserve. The effective Δf_{ENBW} for our configuration was thus determined experimentally as follows. A 1-MΩ resistor was connected to the headstage input as an external noise source. The command voltage was kept at 0 mV (no sine wave). The current monitor output was connected to the lock-in input, and the lock-in outputs were sampled by the computer as in regular capacitance measurements. The spectral current noise density of a 1-MΩ resistor at room temperature (Johnson noise) is $S_I = 1.63 \times 10^{-26}$ A^2/Hz, which is at least two orders of magnitude larger than the instrumental noise, even at high frequencies. Voltage fluctuations at the current-voltage converter input will also cause current fluctuations in the resistor. These voltage fluctuations have an amplitude $e_n \approx 2$ nV $Hz^{-0.5}$ (Sigworth, 1995). The resulting current noise spectral density of 4×10^{-30} A^2/Hz is negligible. Noise measured in this configuration is thus dominated by the Johnson noise of the resistor.

The fluctuations in the capacitance trace were converted into current fluctuations, using Eq. 2, and the current variance at the headstage input σ_I^2 was calculated as the sum of the variances of the two lock-in outputs. The equivalent noise bandwidth was then obtained from the relation

$$\Delta f_{ENBW} = \frac{\sigma_I^2}{S_I}, \quad (4)$$

which was determined to be 30 Hz ± 10%, close to the theoretical value of 25 Hz.

RESULTS

Instrumental noise

The instrumental noise was determined by making capacitance measurements with open headstage input. Fig. 1 *A* shows the instrumental capacitance noise levels measured with the EPC-7 and the EPC-9, respectively. With our EPC-9 model the noise in the two lock-in outputs showed a phase dependence above 20 kHz when the sine wave was on. We therefore varied the phase in the analysis, optimizing for maximum and minimum noise in the two traces (Fig. 1 *B*). The resulting phase was not correlated to the phase of the compensation. This effect was only seen with the sine wave switched on. Because of this unexplained behavior most measurements were made with the EPC-7 amplifier. For the EPC-7 we also determined the noise with the sine wave turned off. It was indistinguishable from that determined with the sine wave on (data not shown).

The current noise spectral density increases with frequency (Sigworth, 1995). This behavior is also observed in measurements with a lock-in amplifier (Fig. 1 *C*). The signal amplitude, however, also increases with frequency. The signal amplitude expressed as the change in pipette current

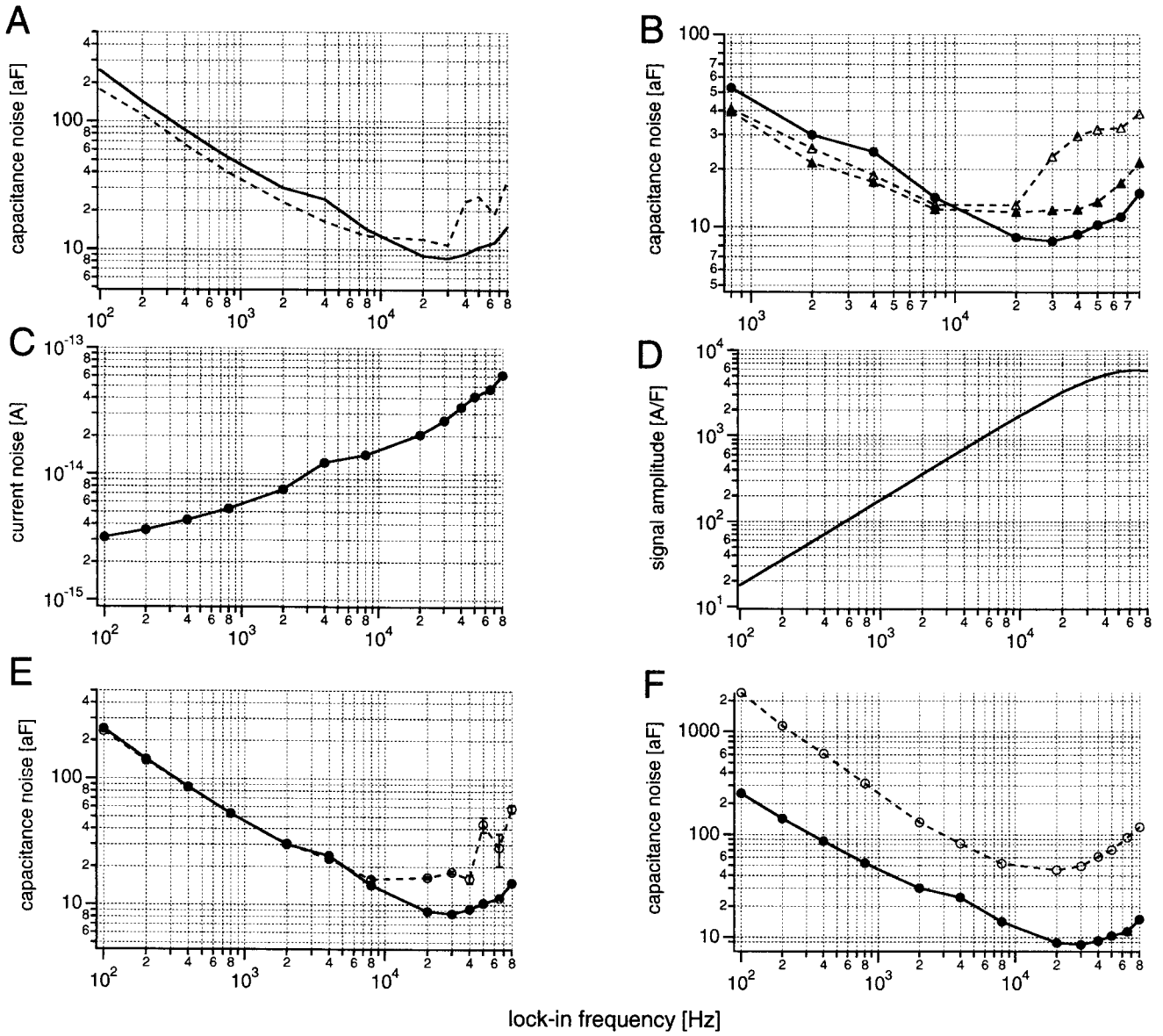

FIGURE 1 Amplifier noise measurements with 20-mV rms sine wave. (*A*) Amplifier noise (open headstage) calibrated in capacitance units for the EPC-7 (——) and the EPC-9 (– – –) as a function of frequency. (*B*) Noise measured with the EPC-9 was found to be phase dependent. Shown are the maximum (– – –, △) and minimum (– – –, ▲) noise, scaled in aF, compared to the noise of the EPC-7 (——, ●). Note the different scale on the frequency axis. (*C*) Frequency dependence of current noise as measured in the capacitance channel with the lock-in amplifier. The noise at the lock-in output was converted into current noise, using Eq. 2. It should be noted that this reflects only half the current variance, inasmuch as noise is not a synchronous signal. (*D*) Theoretical signal amplitude (Eq. 5) for a patch time constant $\tau = 2.4$ μs. (*E*) Capacitance noise measured with the EPC-7 with the internal 10-kHz F1 filter off (——, ●) and on (– – –, ○). (*F*) Comparison of the capacitance noise in the high-gain range (——, ●) and low-gain range (– – –, ○) (EPC-7).

per change in membrane capacitance is, according to Eq. 1,

$$\frac{\Delta I_{\text{pip}}}{\Delta C_{\text{M}}} = \frac{2\pi f}{1 + (2\pi f\tau)^2}\, V_0. \tag{5}$$

The signal amplitude thus increases linearly with f up to the corner frequency $f_{\text{C}} = 1/2\pi\tau$, which for $\tau = 2.4$ μs gives $f_{\text{C}} = 66.3$ kHz (Fig. 1 *D*). Below 10 kHz (EPC-9) and 30 kHz (EPC-7), the increase in signal amplitude supersedes the increase in the current noise.

The resulting capacitance noise thus decreases up to a frequency of ~10 kHz (Fig. 1 *E*). Above this frequency the noise level is rather flat, having a value of ~10 aF for the EPC-7, providing a wide range of frequencies with low instrumental noise. At these high frequencies, however, the patch-clamp amplifier is easily saturated, because small

capacitance changes produce large changes in pipette current. Taking a maximum peak-to-peak output range of ±10 V for the patch-clamp amplifier corresponds to an rms value of $(10/\sqrt{2})V$ for a sine wave signal. Using Eq. 1, the maximum capacitance change ΔC_{max} can be calculated as

$$\Delta C_{max} = \frac{10V}{\sqrt{2}V_0\omega|T(\omega)|^2 Gt(f)}.$$

Fig. 2 shows the measuring range ΔC_{max} for $V_0 = 20$ mV rms, and a gain G of 50 mV/pA. ΔC_{max} decreases linearly up to ~30 kHz, where the $|T(\omega)|^2$ term limits the size of the capacitive current. It can be seen that even for a gain of 50 mV/pA, which is the lowest gain in the high-gain range for both the EPC-7 and the EPC-9, a capacitance change of ~100 fF would drive the patch-clamp amplifier into saturation at frequencies above 10 kHz. For higher sine wave amplitudes V_0, the capacitance bandwidth ΔC_{max} is proportionally smaller.

This problem can be overcome by using the internal 10-kHz output filter of the EPC-7 amplifier. Because the filter is located before the last amplification stage (Sigworth, 1995), switching in the filter increases the capacitance measuring range (Fig. 2, *dashed line*). With the 10-kHz filter on, capacitance changes of at least 150 fF can be detected at all frequencies.

Noise from sources preceding the filter (e.g., headstage input, feedback resistor, patch) should be suppressed by the same amount as the signal, such that the SNR should ideally not be affected by switching in the filter. Noise sources subsequent to the filter, however, now contribute relatively more strongly. The open headstage noise with the output filter set at 10 kHz is shown in Fig. 1 *E* (*open symbols*). It was found that under these conditions the noise at the lock-in output was somewhat different for the two channels above 40 kHz. Presumably, this asymmetry was due to very small signal levels (less than 1 mV at the lock-in output).

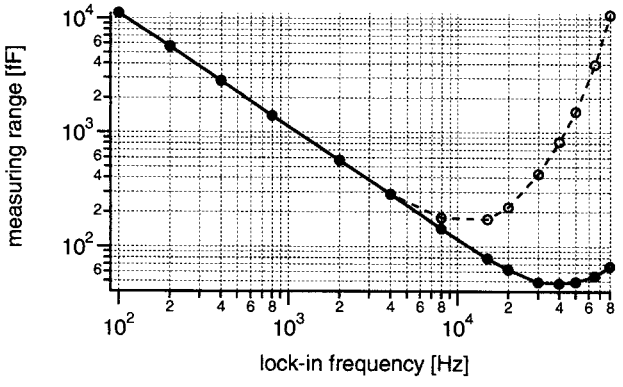

FIGURE 2 Capacitance measuring range as a function of frequency for 20-mV (rms) sine wave. Amplifier gain, 50 mV/pA. ——, 10 kHz, filter off; – – –, 10 kHz, filter on.

Another means of increasing the measuring range is to select a lower gain at the patch-clamp amplifier. Below 50 mV/pA, however, the 500-MΩ rather than the 50-GΩ feedback resistor is used, resulting in a ~10-fold increased instrumental noise. The noise in the low-gain range is shown as open circles in Fig. 1 *F*, compared to the open headstage noise in the high-gain range (*filled circles*).

Phase adjustment in cell-attached recording conditions

To determine the capacitance noise in actual recording conditions, capacitance measurements were carried out in the cell-attached mode, using cells from the neuroblastoma-glioma NG 108-15 cell line. Fig. 3 *A* shows traces recorded with a 65-kHz sine wave. The phase was adjusted to the phase of the calibration. Steps are restricted to the *C* trace and flickers to the *G* trace, indicating that the phase was properly adjusted. However, small phase errors leading to small projections in the *G* trace would be undetectable because of the small size of the capacitance steps in this recording.

Fig. 3 *B* shows traces from the same patch recorded with a 50-kHz sine wave. In this recording larger capacitance steps occurred in the *Y*2 trace, and small projections are visible in the *Y*1 trace. After the phase of the traces is shifted by −16°, they become confined to the *C* trace, and the *G* trace is flat. By adjusting the phase such that capacitance steps appear only in the *C* trace and produce no projection in the *G* trace, the phase and therefore the time constant of the patch can be determined. This method assumes that capacitance steps reflect exo- or endocytotic events. Phase adjustments were performed with this method, using sine wave frequencies of 50, 65, and 80 kHz. High frequencies were chosen, because at low frequencies $\omega\tau$ becomes very small and the phase angle therefore becomes practically zero. From measurements on six patches with different frequencies we obtained an average time constant of 2.4 ± 0.7 μs (SD_n, $n = 15$).

Another means of adjusting the phase is to apply gentle suction to the pipette. This manipulation causes transient capacitance changes as the patch is sucked reversibly up into the pipette (Fig. 4). With the initial phase setting projections occur in the *G* trace. These could be eliminated by a 23° phase shift. From this value we estimate a time constant of 3 μs for this particular patch.

Noise in cell-attached recording conditions

Fig. 5 (*top*) shows average capacitance noise levels from measurements on seven patches at various frequencies between 800 Hz and 80 kHz (*solid line*). Noise levels of 40 aF or less could be routinely obtained above 8 kHz with the 20-mV rms sine wave amplitude used here. This allows us

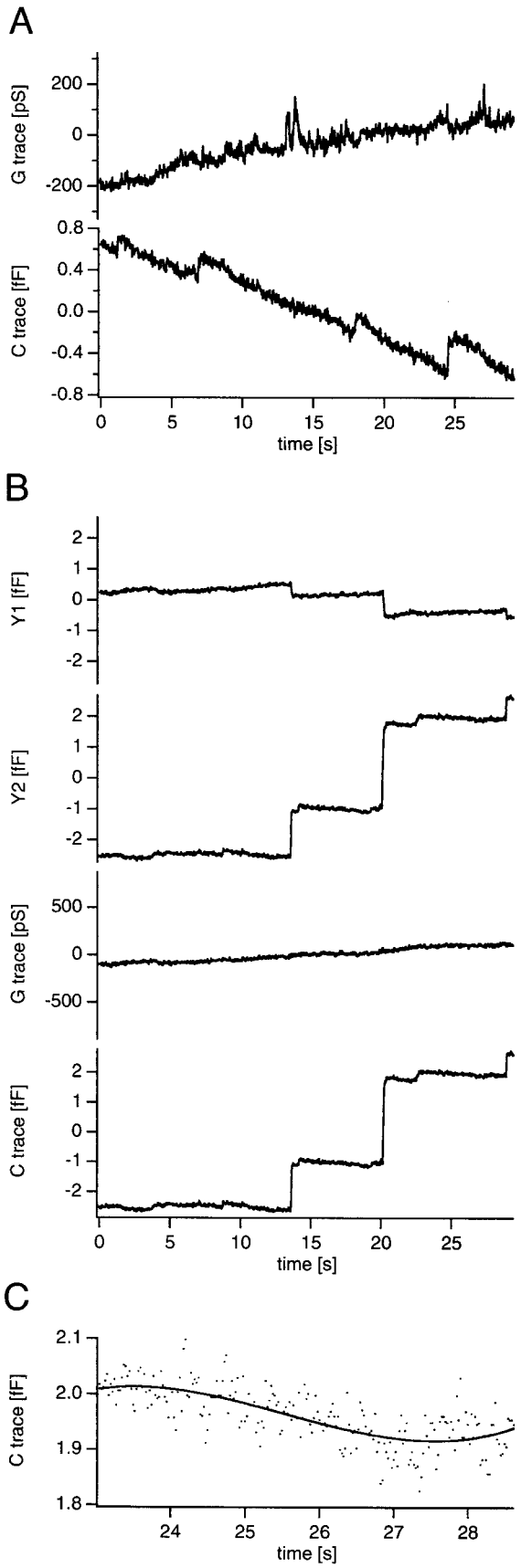

to detect exo- and endocytosis of vesicles with a 160-aF capacitance or a 70-nm diameter. For comparison capacitance noise was recorded with the same pipettes, with the pipette positioned just above the bath (*dashed line*). This noise is a factor of ~2–3 smaller.

Because the measuring range is, as mentioned before, very small at high frequencies, three of the seven patches were also measured with the internal 10-kHz filter of the EPC-7 on, using lock-in frequencies between 8 and 80 kHz. The middle panel of Fig. 5 shows the average capacitance noise in these three patches with the filter on (*dashed line*) and off (*solid line*). With the 10-kHz filter the noise is increased, especially at frequencies of 50 kHz and higher. This presumably reflects contributions from noise sources in the signal path located within or subsequent to the 10-kHz low-pass filter.

In four patches, the capacitance noise was determined with the sine wave on and off. When the sine wave is off, fluctuations from the patch parameters do not contribute to the noise. The bottom panel of Fig. 5 shows the average capacitance noise with the sine wave off (*dash-dotted line*), in comparison with the average capacitance noise with the sine wave on (*solid line*). The measurements with the sine wave off were calibrated in Farads, assuming the same 20-mV rms sine wave amplitude. Although the error bars indicating the scatter of individual measurements overlap, the noise with the sine wave off is systematically lower than the noise with the sine wave on. This is further supported by the fact that in 33 of 38 measurements for individual patches and frequencies, the noise recorded with the sine wave off was smaller than the noise with the sine wave on.

Noise measurements with open headstage did not show a dependence on the sine wave amplitude. This suggests that the additional noise with the sine wave on may result from small fluctuations of the patch capacitance or of parasitic capacitances. If this were indeed the case, then the current noise would increase with increasing sine wave amplitudes. The "extra capacitance noise" should contribute more at higher amplitudes such that the capacitance noise level does not decrease with the inverse of the amplitude, as would be expected if the noise were independent of the sine wave amplitude. To test this hypothesis, we performed noise measurements on five patches, using sine wave frequencies of 800 Hz, 8 kHz, 20 kHz, and 40 kHz, with sine wave amplitudes of 0 mV (sine off), 20 mV rms, 50 mV rms, 70

FIGURE 3 Capacitance recordings in cell-attached configuration. All measurements are from the same cell. (*A*) 65-kHz sine wave. Small capacitance steps and seal flickers appear to be well separated at the phase of the compensation. (*B*) 50-kHz sine wave. Larger capacitance steps are accompanied by small projections in the conductance trace (*upper panels*). After a phase shift of −16°, the *G* trace is flat. (*C*) Part of the *C* trace shown in *B* on an expanded scale, together with a polynomial fit to determine the noise level.

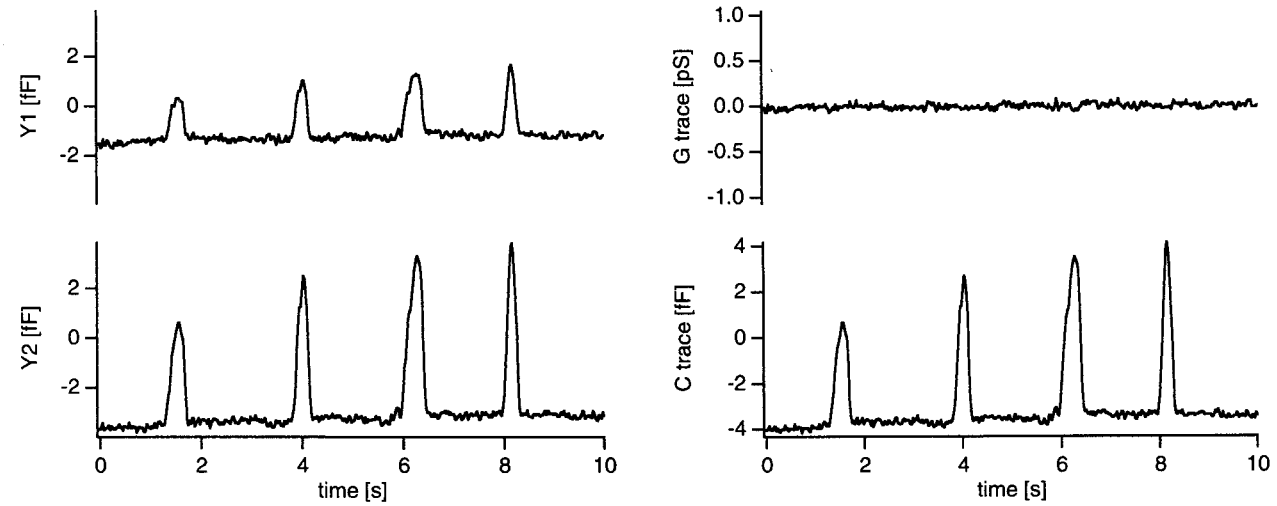

FIGURE 4 Cell-attached capacitance measurements, using 40-kHz sine wave with suction pulses applied to the pipette for phase adjustment. Shown are the traces at the phase of the compensation (*left*) and after a phase shift of 23° (*right*).

mV rms, and 100 mV rms. To avoid saturation in the EPC-7 due to the large sine wave amplitudes, the internal 10-kHz F1 filter in the EPC-7 was switched on for all measurements.

Fig. 6, *A* and *B* shows the current noise measured at the phase of capacitance changes. As in Fig. 1 *C*, this reflects only half of the current variance at the headstage input. Unexpectedly, the current noise increases with the sine wave amplitude for all four frequencies. With the 100-mV sine wave the noise is about two times higher than in the absence of the sine wave. Consequently, the capacitance noise in a recording with 100-mV sine wave amplitude was not five times smaller than that in a recording with 20-mV amplitude (Fig. 6 *C*). The mean reduction in noise was only about threefold, giving a rms noise level of 12–15 aF at 100 mV rms amplitude between 8 and 40 kHz.

The "extra noise" that depends on the applied sine wave was estimated by subtracting the variance measured with the sine wave off from the corresponding variance with the sine wave on, assuming that the two noise sources are not correlated. The extra current noise, i.e., the square root of the extra variance, is plotted as a function of frequency in Fig. 6 *D* for sine wave amplitudes of 50 and 100 mV. The data points for the two amplitudes show a similar frequency dependence but differ by a factor of ~2. The extra current noise thus appears to be proportional to the sine wave amplitude.

When the current noise is converted into capacitance noise, the data points measured with the 100-mV sine wave are in very good agreement with those measured at 50-mV amplitude (Fig. 6 *E*). It should be noted that for 100-mV amplitude the extra noise is the dominant noise source and is practically equal to the total capacitance noise shown in Fig. 6 *C*. The extra capacitance noise is markedly increased at 800 Hz, suggesting that the extra capacitance noise is not simply reflecting slow fluctuations of a linear capacitance.

Fig. 7 compares our results to previous studies of noise in patch recordings. The upper panel shows the current noise spectral density, the lower panel the capacitance noise for a sine wave of 20-mV rms amplitude. Our data points (*open circles*) were obtained from the lock-in measurements. The variance measured in the lock-in capacitance channel was converted into a current variance and multiplied by a factor of 2 to take into account that the lock-in splits up the asynchronous noise into the two channels. The current noise spectral density was obtained from the variance and the equivalent noise bandwidth, using Eq. 4. Our data points are close to the spectral current noise density measured in mouse fibroblasts by Sigworth and co-workers (*filled circles*) (Sine et al., 1990; Sigworth, 1995). The solid line shows an estimate of the theoretical limit that is possibly achievable in the cell-attached configuration, taking into account the instrumental noise and contributions from other noise sources, such as noise from the patch itself and dielectric loss (see Appendix). This estimate is in good agreement with the measurements, indicating that the noise level obtained in our recordings approaches the optimal resolution attainable with a resistor-feedback amplifier and standard pipettes. At high frequencies the measured noise was actually slightly smaller than the theoretical estimate, suggesting that for this patch τ_{patch} was slightly smaller than 1.4 μs or R_A slightly higher than 5 MΩ, as assumed in the theoretical estimate.

The use of a capacitive feedback amplifier and heavily coated quartz pipettes can significantly reduce the noise in cell-attached recordings, as demonstrated by Levis and Rae (1993). A noise estimate based on their data is given as the

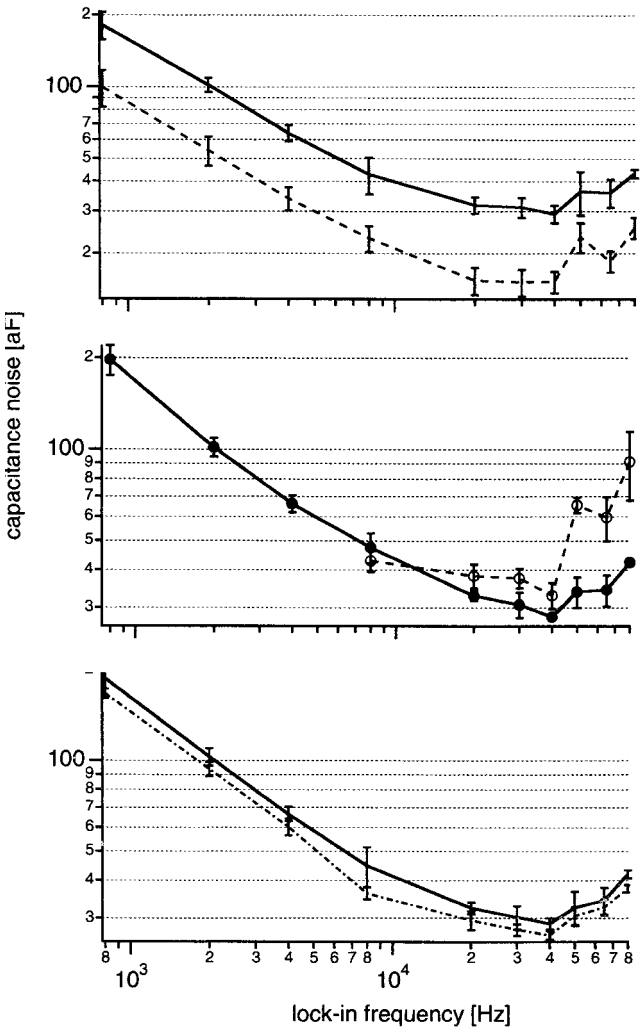

FIGURE 5 Capacitance noise in the cell-attached configuration. (*Top*) Noise in cell attached (——) and with the respective pipette suspended freely directly over the bath (– – –). Values are mean ± SD_n from seven cells. (*Middle*) Subset of three patches, on which the capacitance noise in the cell-attached configuration was also measured with the 10-kHz F1 filter on (– – –, ○), compared to the values with the filter off (——, ●). (*Bottom*) Subset of four patches on which the capacitance noise was also measured with the sine wave off (– · – · –).

dashed line in Fig. 7. The spectral current noise density is calculated from that measured by Levis and Rae with a pipette attached to a sylgard layer at the bottom of the recording chamber plus theoretical noise from the patch added. Here we assumed a patch with $C_{patch} = 0.1$ pF and $R_A = 2$ MΩ. These optimal recording conditions should reduce the noise to ≤7 aF above 20 kHz, even with a 20-mV rms sine wave. This would allow for the resolution of 30-nm vesicles as single capacitance steps.

Resolution of fusion pores

Low-noise capacitance measurements are not only important for the reliable measurement of small capacitance steps. A low noise level is also essential for measuring the fusion pore conductance over a wide range of conductance values as previously described for whole-cell recordings (Curran et al., 1993). Changes in the imaginary part of the admittance (Im) are usually indicated by one of the lock-in outputs (*Y*2) and reflect capacitance changes, whereas changes in the real part (Re) indicated by the other output (*Y*1) reflect conductance changes. However, when the fusion pore connecting the vesicle to the extracellular space is included in the equivalent circuit analysis (Breckenridge and Almers, 1987), then the fusion pore conductance (G_P) and vesicle capacitance (C_V) are related to the changes Re and Im according to

$$C_V = \frac{1}{2\pi f}\frac{\mathrm{Re}^2 + \mathrm{Im}^2}{\mathrm{Im}}$$

$$G_P = \frac{\mathrm{Re}^2 + \mathrm{Im}^2}{\mathrm{Re}}$$

(Lindau, 1991; Lollike et al., 1995). The noise in the calculated fusion pore conductance may then be expressed as

$$\Delta G_p = \sqrt{\left(\frac{\partial G_p}{\partial \mathrm{Re}}\Delta\mathrm{Re}\right)^2 + \left(\frac{\partial G_p}{\partial \mathrm{Im}}\Delta\mathrm{Im}\right)^2},$$

where ΔRe and ΔIm denote the noise levels of Re and Im, respectively. For stable recordings we may assume that the noise is similar in the two lock-in channels: ΔRe = ΔIm =: $\omega\Delta C$, where ΔC is the capacitance noise as described above.

With Im/Re = $G_P/\omega C_V$ the noise in the fusion pore conductance values can be written as

$$\Delta G_P = \left(1 + \left(\frac{G_P}{\omega C_V}\right)^2\right)\omega\Delta C, \qquad (6)$$

and the signal-to-noise ratio at which the fusion pore conductance is obtained (SNR_P) is accordingly given by

$$\mathrm{SNR}_P(G_P, C_V) := \frac{G_P}{\Delta G_P} = \frac{G_P/\omega\Delta C}{1 + (G_P/\omega C_V)^2}. \qquad (7)$$

For any given vesicle size the best SNR_P is obtained at $G_P = 2\pi f C_V$. To obtain reliable estimates of G_P, however, it is necessary to follow G_P over a certain range in which SNR_P is sufficient. Fig. 8 shows isocontour plots for $SNR_P = 4$ and $SNR_P = 10$ (Eq. 7) as a function of fusion pore conductance G_P and vesicle capacitance C_V for lock-in frequencies of 8, 20, and 50 kHz. We assumed that $\Delta C = 15$ aF, as can be routinely obtained for the given frequencies and 100-mV rms amplitude. For $G_P \ll \omega C_V$ the noise in the fusion pore determination approaches a constant value $\omega\Delta C$ (Eq. 6), giving a lower limit for the detection of the fusion pore that increases from 3 pS at 8 kHz to 19 pS at 50 kHz. However, this also sets a limit with respect to the minimum size of the vesicle. For large fusion pore conductances the noise increases proportionally to G_P^2, while the signal am-

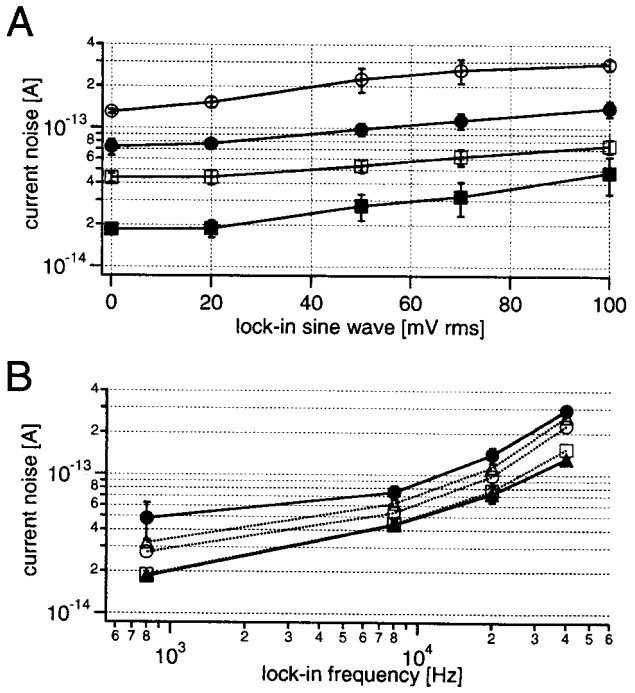

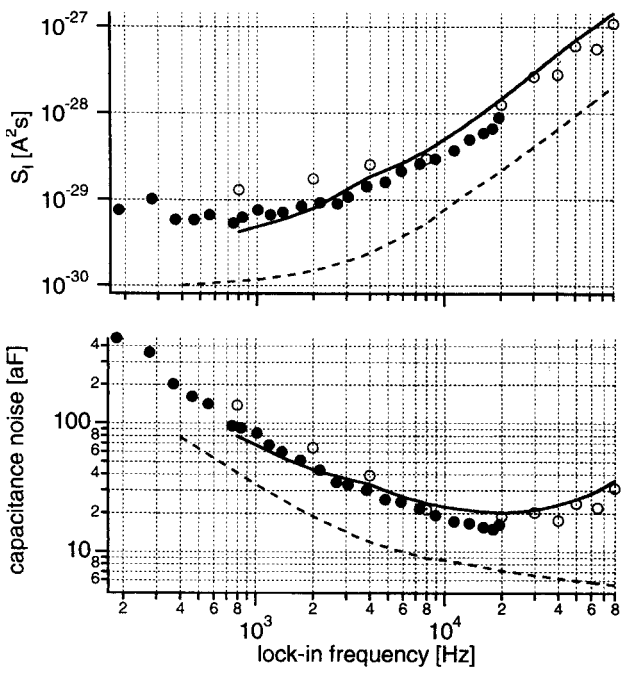

FIGURE 7 Comparison of the noise levels determined with the lock-in amplifier to previous noise measurements given in the literature. ○, Best patch from our lock-in measurements. ●, Data from Sine et al. measured in mouse fibroblasts (Sigworth, 1995). ——, Theoretical estimate of noise in cell-attached recordings as described in the Appendix. – – –, Noise spectrum estimated for quartz pipettes and capacitive feedback as described by Levis and Rae (1993), assuming $R_A = 2$ MΩ and $C_{patch} = 0.1$ pF. (*Top*) Spectral current noise density. (*Bottom*) Conversion into capacitance noise, assuming 20-mV sine wave amplitude.

plitude grows only linearly with G_P. This gives an upper limit for the resolution of the fusion pore.

The range in which the fusion pore can be detected with at least a given signal-to-noise ratio SNR_P^* can be estimated quite easily. For a given angular frequency ω and a given vesicle size C_V, one can calculate from Eq. 7 the two values for G_P where the signal-to-noise ratio equals SNR_P^*:

$$G_P^{1,2} = (\omega C_V)\left[\frac{C_V}{2SNR_P^*\Delta C} \pm \sqrt{\left(\frac{C_V}{2SNR_P^*\Delta C}\right)^2 - 1}\right].$$

In terms of the signal-to-noise ratio for a particular capac-

FIGURE 6 Dependence of noise on sine wave amplitude. All measurements were performed with the 10-kHz filter on. (*A*) Data points are for 800 Hz (■), 8 kHz (□), 20 kHz (●), 40 kHz (○). (*B–E*) Frequency dependence of noise for different sine wave amplitudes. rms amplitudes were 0 (▲), 20 (□), 50 (○), 70 (△), and 100 mV (●). (*B*) Measured noise, converted to current noise at headstage input. (*C*) Capacitance noise for 20-, 50-, and 100-mV amplitudes. (*D*) Extra current noise due to applied sine wave for 50- and 100-mV amplitudes (see text). (*E*) Extra capacitance noise for 50- and 100-mV amplitudes.

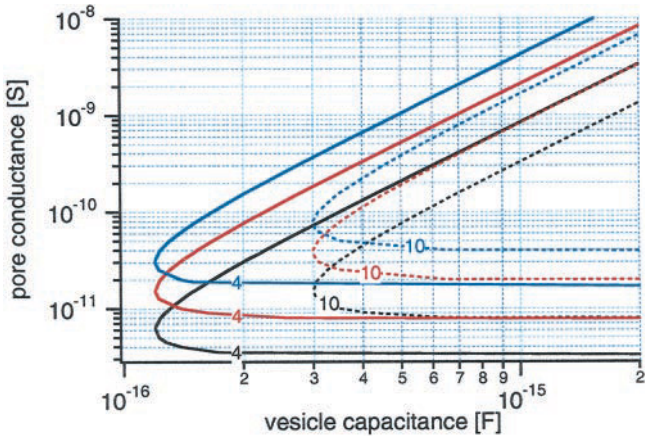

FIGURE 8 Isocontour plots of theoretical signal-to-noise ratio in fusion pore determinations as a function of vesicle capacitance and pore conductance. Calculations were for lock-in frequencies of 8 (*black*), 20 (*red*), and 50 kHz (*blue*). Lines are for a SNR = 4 (——) and SNR = 10 (– – –). Calculations are based on Eq. 7, assuming capacitance noise $\Delta C = 15$ aF.

itance step $\mathrm{SNR_C} = C_V/\Delta C$, this may also be expressed as

$$G_P^{upper} = \omega C_V\left[\frac{\mathrm{SNR_C}}{2\mathrm{SNR_P^*}} + \sqrt{\left(\frac{\mathrm{SNR_C}}{2\mathrm{SNR_P^*}}\right)^2 - 1}\right]$$

$$G_P^{lower} = \omega C_V\left[\frac{\mathrm{SNR_C}}{2\mathrm{SNR_P^*}} - \sqrt{\left(\frac{\mathrm{SNR_C}}{2\mathrm{SNR_P^*}}\right)^2 - 1}\right].$$

Obviously, $\mathrm{SNR_C}$ has to be $>2\mathrm{SNR_P^*}$. For $\mathrm{SNR_C} > 3\mathrm{SNR_P^*}$ we may approximate with an error of less than 15%:

$$G_P^{lower} \approx \omega C_V \frac{\mathrm{SNR_P^*}}{\mathrm{SNR_C}} \quad \text{and} \quad G_P^{upper} \approx \omega C_V \frac{\mathrm{SNR_C}}{\mathrm{SNR_P^*}}.$$

With a capacitance noise of 15 aF and a desired $\mathrm{SNR_P^*} = 4$, this approximation holds for vesicles with $C_V > 180$ aF. These formulas may also be rewritten in terms of C_V and ΔC, giving

$$G_P^{lower} \approx 4\omega\Delta C \tag{8}$$

$$G_P^{upper} \approx \frac{1}{4}\,\omega\,\frac{C_V^2}{\Delta C}. \tag{9}$$

Early fusion pore conductances have mean values around 250 pS, with most pores being in the range of 35–700 pS (for a review see Lindau, 1998). To measure fusion pore conductances as low as 35 pS at a noise level in the two traces equivalent to 15 aF rms, Eq. 8 implies that we must choose a sine wave frequency below 90 kHz. Even for noise levels of 25 aF, all frequencies below 50 kHz may be used. To measure pore conductances as large as 700 pS, Eq. 9 gives

$$C_V > 2 \cdot \sqrt{\frac{\Delta C \cdot 700\ \mathrm{pS}}{\omega}}. \tag{10}$$

To measure large pore conductances in small vesicles we should choose the highest possible frequency. As we have shown, low capacitance noise may be obtained up to at least 50 kHz. With $\Delta C = 15$ aF, Eq. 10 gives $C_V > 370$ aF for 50 kHz. This corresponds to vesicles with ~110–120-nm diameter.

DISCUSSION

Single exocytotic fusion events can be investigated in great detail by the use of time-resolved capacitance measurements. Most of these studies were performed using the patch-clamp whole-cell configuration (for a review see Lindau, 1991). However, the resolution of single events is limited particularly by the Johnson noise of the access resistance, which is transmitted via the high capacitance of the whole-cell membrane (Lindau and Neher, 1988; Gillis, 1995). Exocytosis of small vesicles can be measured at improved resolution in the cell-attached configuration (Neher and Marty, 1982; Lollike et al., 1995, 1998; Albillos et al., 1997; Kreft and Zorec, 1997). As for the studies of single ion channels (Hamill et al., 1981), the reduced noise in patch recordings can thus also be exploited to study the fusion of small vesicles.

The method we use for patch capacitance measurements was originally introduced by Neher and Marty (1982) and is similar to the piecewise-linear technique as used in whole-cell capacitance measurements (Neher and Marty, 1982; Fidler and Fernandez, 1989; Lindau and Neher, 1988; Gillis, 1995). In whole-cell recordings two important technical aspects have been considered: the determination of the correct phase where changes in capacitance and conductance are well separated (Neher and Marty, 1982; Fidler and Fernandez, 1989; Lindau and Neher, 1988; Debus et al., 1995; Gillis, 1995) and the choice of the sine wave frequency where the best SNR is obtained (Neher and Marty, 1982; Lindau and Neher, 1988; Gillis, 1995).

Phase adjustment

As in whole-cell recordings, the phase at which conductance and capacitance changes are separated is important. For whole cell capacitance measurements various techniques have been proposed. The Neher-Marty technique (also called the piecewise-linear technique) uses "capacitance dithering," where the value of the slow capacitance compensation is changed and the phase is adjusted such that no changes are observed in the conductance trace (Neher and Marty, 1982). This method requires that the compensation be very well adjusted. In the Lindau-Neher technique (Lindau and Neher, 1988) the DC current is measured as a third parameter that allows the calculation of all equivalent circuit parameters, provided that a reasonable estimate of the reversal potential is available. This method requires that

the fast capacitance be very well compensated. Methods with two sine waves do not require knowledge of the reversal potential but still require accurate compensation of parasitic capacitances (Rohlicek and Rohlicek, 1993; Donelly, 1994; Rohlicek and Schmid, 1994; Barnett and Misler, 1997). The "phase tracking" or "resistance dithering" technique (Fidler and Fernandez, 1989) determines the phase from the changes that occur when a resistor is switched between the bath electrode and a ground. This method suffers from limitations, mostly from the fast capacitance between recording electrode and bath, as well as from large conductances in the cell membrane (Debus et al., 1995; Gillis, 1995).

For patch recordings only the original Neher-Marty technique seems to be practical. The reason for this is that the patch capacitance is small and the separation from other stray capacitances is a difficult procedure (Sakmann and Neher, 1983). All of the automatic methods described above require that the quantity of interest, the membrane capacitance, can be well separated from stray capacitances by its time constant.

As in the case of whole-cell recordings, the correct phase depends on the time constant for charging the patch. We determined experimentally an average time constant of 2.4 ± 0.7 μs. This appears to be rather slow, because patch capacitances C_P are roughly proportional to pipette resistance (Sakmann and Neher, 1983):

$$C_P \approx \frac{126fFM\Omega}{R_P},$$

which would give a time constant of 0.126 μs. However, we must keep in mind that in the above relation R_P is the pipette resistance before the seal is made. In the cell-attached configuration the patch is Ω-shaped (Sakmann and Neher, 1983), and the series resistance of the pipette tip is accordingly located between the patch and the intracellular space. This implies a different conductivity and furthermore means that the tip may be partially obstructed by cellular organelles. In addition, the pipette capacitance between tip and patch is in parallel with the patch and is charged together with the patch. It should be noted that some patches have time constants well below 1 μs.

As in whole-cell recordings, the phase of the lock-in amplifier where capacitance and conductance changes are well isolated is given by

$$\Phi_T = -2\tan^{-1}\left(\frac{\omega\tau}{1 + G_P R_S}\right).$$

With $G_P R_S \ll 1$ this becomes simply

$$\Phi_T = -2\tan^{-1}(\omega\tau).$$

With $\tau = 2.4$ μs the phase shift is $<2°$ for frequencies below 1 kHz. However, at 8 kHz a phase shift of $\sim 14°$ is estimated, and it increases to 100° at 80 kHz. An approximate phase setting is obtained with the capacitance compensation with a time constant of ~ 1.9 μs. However, at high frequencies the actual phase of the patch capacitance changes may be quite different. The correct phase is best determined from the recording itself and must thus be adjusted off-line. This phase adjustment may be made by minimizing the projections from capacitance changes into the conductance trace or form conductance changes into the capacitance trace. Pure capacitance changes may be produced artificially by suction pulses, and these can then be used to set the phase. Alternatively, ion channel openings or capacitance steps due to exo- or endocytosis may be used to find the correct phase. A correct phase setting is of particular importance for the determination of fusion pore conductances.

Capacitance noise

Previous studies of noise in patch recordings had been focused on current noise for single-channel recordings (Benndorf, 1995; Levis and Rae, 1998). For single-channel measurements, the noise usually comes from a broad frequency range (typically some kHz) with a lower limit of 0 Hz (DC). In contrast, high-resolution capacitance measurements with a lock-in amplifier use a sine wave command voltage and a narrow bandwidth detection method (Neher and Marty, 1982; Joshi and Fernandez, 1988; Lindau and Neher, 1988; Gillis, 1995). The bandwidth in these measurements is usually only some 10 Hz, centered around the sine wave frequency. Furthermore, the signal amplitude in single-channel recordings does not depend on frequency, as do capacitive currents.

In the case of whole-cell measurements, the Johnson noise of the access resistance is the dominant noise source, and instrumental noise is negligible (Lindau and Neher, 1988; Gillis, 1995). In the cell-attached configuration, several noise sources must be considered. These include noise generated within the amplifier, the noise of the seal conductance and patch, noise picked up by the recording pipette, and noise produced within the pipette material. Above some 100 Hz the current noise density generally increases with increasing frequency (Hamill et al., 1981; Sigworth, 1995). This is true for instrumental noise as well as noise in actual cell-attached recordings. However, in capacitance measurements with sine wave excitation the signal increases in proportion to the sine wave frequency, and this increase outweighs the increase in noise. The resulting capacitance noise thus decreases with frequency up to 30 to 50 kHz and then increases slightly toward 80 kHz. This rise at very high frequencies comes from the frequency dependence of the signal amplitude due to the patch time constant and may not be present in patches with very small time constants. With our experimental conditions and a sine wave of 20 mV rms, we obtained a capacitance noise of 30–40 aF between 8 and

80 kHz. A noise level of 30 aF allows for the reliable detection of 60-nm vesicles.

The noise levels we determined experimentally are close to the theoretical limits for patch recordings. At high frequencies the noise is mainly generated by the patch configuration itself. The noise of the patch can be estimated by using the Nyquist formula

$$S_D = 4kT \cdot \mathrm{Re}(Y_P),$$

with

$$\mathrm{Re}(Y_P) = G_L + \frac{(2\pi f \tau_{patch})^2}{R_A[1 + (2\pi f \tau_{patch})^2]}$$

(see Appendix). At high frequencies (≥6 kHz) this is the dominant noise source. Accordingly, patches with small capacitance and low access resistance will have the lowest possible noise, just as in whole-cell recordings.

Because the patch-clamp amplifier is easily saturated at these high frequencies, we also determined the noise level with the EPC-7 10-kHz output filter switch on. This filtering increases the noise somewhat, giving a noise level of 40 aF between 8 and 40 kHz, rising to 90 aF at 80 kHz. A noise of 40 aF still allows for the detection of 70-nm vesicles.

There are several possible ways to further decrease the capacitance noise level. One possibility is to decrease the equivalent noise bandwidth by stronger filtering of the lock-in outputs. The drawback is a significantly slower step response time. Another possibility is an increase of the sine wave amplitude to 50 mV (Lollike et al., 1995, 1998) or even >100 mV (Kreft and Zorec, 1997). Generally, a 100-mV rms sine wave can be routinely used in cell-attached measurements, and for stable seals, a sine wave of even 200 mV rms is possible (Henkel and Almers, unpublished observations). With 100 mV rms, capacitance noise as low as 14 aF could be obtained between 8 and 40 kHz. This allows for the detection of 45-nm vesicles as capacitance steps.

Interestingly, the noise measured at the lock-in output was found to depend on the sine wave amplitude, and at 100 mV the voltage-dependent contribution is the dominant noise source, at least in the 0.8–40-kHz range. This "extra current noise" was not observed in measurements with an open headstage, indicating that it may reflect properties of the pipette, seal, or patch. The extra capacitance noise scales linearly with the sine wave amplitude, as would be expected from unresolved capacitance fluctuations in the patch. However, the extra noise shows a marked frequency dependence. It increases about fivefold at 800 Hz compared to the 8–40-kHz range. Such a frequency dependence would not be expected for fluctuations in patch capacitance in the frequency range below 15 Hz, which are picked up by the lock-in amplifier with the filter settings used here. However, when a sine wave voltage is applied to a fluctuating capacitance, current frequency components are generated not only at the sum but also at the difference of sine wave frequency and fluctuation frequency. The low frequency fluctuations produce frequencies slightly above or below the sine wave frequency in the sum component. Additionally, the lock-in amplifier will pick up fluctuation frequencies slightly above or below a value twice the sine wave frequency, because these will generate frequencies near the original sine wave frequency in the difference component. The decrease in the extra noise between 800 and 8000 Hz may thus possibly reflect a frequency dependence of capacitance fluctuations. If the amplitude of capacitance fluctuations decreases strongly between 1.6 and 16 kHz, then the measured capacitance noise should decrease between 800 and 8000 Hz, as observed. The physical basis for this "extra noise" has not yet been fully explored. Whatever the underlying mechanism is, the resulting extra capacitance noise is independent of the sine wave amplitude and thus indicates a limitation in noise reduction under the recording conditions employed here.

Fusion pores in small vesicles

Fusion of a secretory vesicle with the plasma membrane begins with the formation of a narrow fusion pore (Breckenridge and Almers, 1987). In vesicles covering a wide range of sizes it was found that initial fusion pore conductances had mean values of 150–330 pS (Lindau and Almers, 1995), and values higher than 700 pS were extremely rare in all cell types studied (Spruce et al., 1990; Hartmann and Lindau, 1995; Lollike et al., 1995). In chromaffin cells the amperometric foot signal is associated with fusion pores with conductances around 400 pS (Albillos et al., 1997; Alés et al., 1999). In whole-cell recordings the initial fusion pore conductance has been measured by recording the current transient charging the granule membrane to the holding potential upon opening of the fusion pore. This makes it possible to study the fusion pore properties during the first millisecond of its existence. However, this method requires giant granules with diameters larger than 1 μm and has been used only on beige mouse mast cells (Breckenridge and Almers, 1987; Spruce et al., 1990) and horse eosinophils (Hartmann and Lindau, 1995). The subsequent expansion of the fusion pore can then be followed by admittance analysis (for a review see Lindau, 1991), which was recently extended to the use of two-frequency techniques (Ratinov et al., 1998). The detectability of fusion pore conductances depends on the sine wave frequency and vesicle size (Curran et al., 1993). The low noise of patch recordings makes it possible to measure fusion pore conductances in comparatively small vesicles because of the high signal-to-noise ratio.

The measurement of charging transients appears not to be very promising, because a 1-fF vesicle will be charged via a 150-pS fusion pore with a time constant as short as ~7 μs.

Furthermore, for a potential change by 100 mV, the total charge transferred by the current transient will be 10^{-16} As, corresponding to 624 elementary charges. Even in patch recordings this is an extremely small charge to detect. It has been possible, however, to determine fusion pore conductances in cell-attached recordings by analysis of lock-in amplifier recordings (Lollike et al., 1995, 1998; Albillos et al., 1997; Alés et al., 1999), using sine wave frequencies of 8–20 kHz.

Here we performed a rigorous analysis of the detectability of fusion pores in patch recordings. In all cell types studied early fusion pore conductances were usually in the range of 35–700 pS. To optimize the detection of fusion pores in this range the sine wave frequency should be chosen to be as high as possible. The disadvantage of using frequencies higher than 40 kHz is that the capacitance compensation becomes very critical and the patch-clamp amplifier saturates at rather small capacitance changes. This problem may be overcome by switching in the internal filter that precedes the final amplification stage and thus prevents saturation. The resulting reduction in amplitude should in principle be accompanied by a corresponding reduction in noise. Indeed, with a 10-kHz filter the signal-to-noise ratio was hardly affected up to 40 kHz. However, when the frequencies are much higher than the filter frequency the amplitudes become so small that this relation does not hold. It would thus be desirable to use an amplifier equipped with an internal filter with a corner frequency around 30 kHz.

A capacitance noise of 14 aF can be obtained routinely in recordings with a frequency of ~50 kHz. For vesicles with capacitance $C_V > 380$ aF fusion pore conductances between 10 and 700 pS may be resolved with a signal-to-noise ratio greater than 4, provided that the same low noise level is attained in the conductance trace. In our experiments this was indeed the case for most of the recordings. In the range 47–280 pS the signal-to-noise ratio will be >10. A vesicle capacitance of 380 aF corresponds to a vesicle diameter of ~110 nm.

These estimates were obtained with standard techniques. A synaptic vesicle with a 50-nm diameter will have a capacitance of ~80 aF. Fusion pore measurements in such small vesicles require further reduction in the capacitance noise. To measure a pore conductance of 500 pS at a signal-to-noise ratio of 4 would require a 1-aF noise level (Eq. 9). With the EPC-7 patch-clamp amplifier such a noise level has been achieved with open headstage and a 8-kHz, 200-mV rms sine wave. To make smaller vesicles accessible to fusion pore measurements the use of higher frequencies and special low-noise techniques will be required. A reduction in patch time constant may be possible with thick-walled pipettes and would decrease the noise at high frequencies. In addition, the extra capacitance noise, which depends on the sine wave amplitude, has to be reduced.

APPENDIX: NOISE SOURCES IN PATCH RECORDINGS

The noise in the cell-attached configuration comes from various sources: instrumental noise, capacitive load at the headstage input (e_n-C_t noise), distributed RC noise of the pipette, dielectric noise from holder and pipette, and thermal noise from the patch (Benndorf, 1995; Sigworth, 1995; Levis and Rae, 1998). To estimate the theoretical noise levels we measured the instrumental noise with open headstage and estimated theoretical contributions from additional noise sources present in cell-attached recordings as follows.

In the cell-attached configuration, when the pipette is immersed in the grounded bath, an increase in noise is observed because of 1) increased e_n-C_t noise due to the additional fast capacitance, 2) dielectric noise of the holder and pipette, 3) thermal noise contributed from the patch, and 4) distributed RC noise of the pipette.

The spectral density of the e_n-C_t noise S_n is given by

$$S_n = (2\pi f e_n C_t)^2,$$

where $e_n = 2$ nV Hz$^{-1/2}$ and $C_t = 10$ pF for the open headstage (Sigworth 1995). In the cell-attached configuration C_t was increased by ~2 pF compared to the open headstage according to the change in C_{fast} compensation. The increase in e_n-C_t noise is correlated with the instrumental e_n-C_t noise. For uncorrelated noise sources the variances add

$$\sigma^2 = \sum_{i=1}^{n} \sigma_i^2$$

The increase in C_t produces a coherent increase in e_n-C_t noise such that the variance of the total noise becomes

$$\sigma'^2 = \sum_{i=1}^{n-1} \sigma_i^2 + (\sigma_n + \Delta\sigma_n)^2 = \sigma^2 + (2\sigma_n\Delta\sigma_n + \Delta\sigma_n^2),$$

where $(\sigma_n + \Delta\sigma_n)^2$ is the variance due to the e_n-C_t noise in the presence of the increased C_t. Increasing C_t by ΔC_t thus increases the total variance by

$$\Delta\sigma_{Ct}^2 = 2\sigma_n\Delta\sigma_n + \Delta\sigma_n^2.$$

With $\sigma_n = 2\pi f e_n C_t$ and $\sigma_n + \Delta\sigma_n = 2\pi f e_n (C_t + \Delta C_t)$ we get

$$S_{\Delta Ct} = \Delta\sigma_{Ct}^2 = (2\pi f e_n)^2 \cdot [2C_t\Delta C_t + (\Delta C_t)^2].$$

This increase in the variance due to the increased e_n-C_t noise is very small (Fig. 9, *green line*).

The dielectric noise of holder and pipette is difficult to determine because of the complex geometry and the different materials involved. However, most of the contribution comes from the part of the pipette that is immersed in the bath. The dielectric loss factor of the sticky wax was not known. For solid paraffin, we found $D = 0.004$ (Nührmann, 1994), which is close to the loss factor of our glass ($D = 0.005$; Hilgenberg, personal communication). We therefore estimated the dielectric loss with $D = 0.005$ and $C_D = 1.3$ pF, which equals the increase in C_{fast} when the pipette is immersed in the bath. With these parameters the spectral density was obtained with the formula

$$S_D = 4kT2\pi f \cdot D \cdot C_D$$

(Levis and Rae, 1993), where k is the Boltzmann constant and T is the absolute temperature (Fig. 9, *orange line*).

To calculate the distributed RC noise of patch and pipette, we use the Nyquist formula,

$$S_D = 4kT \cdot \mathrm{Re}(Y_P),$$

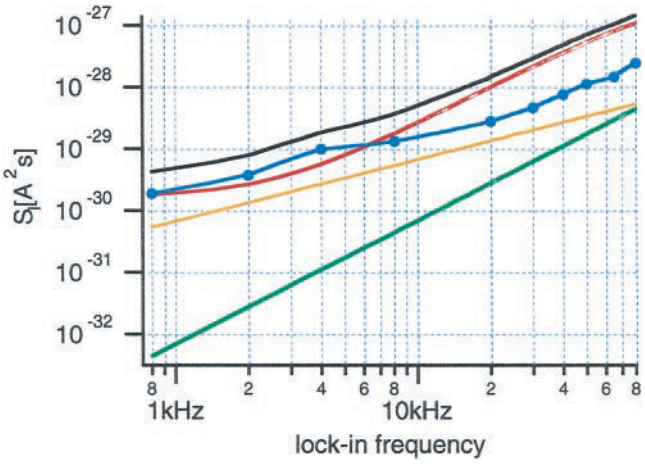

FIGURE 9 Spectral densities of different noise sources contributing to the total noise. Amplifier noise measured with open headstage (*blue*), increase in e_n-C_t noise in the cell-attached configuration (*green*), dielectric noise (*orange*), patch noise (*red*), and total noise (*black*).

where $\mathrm{Re}(Y_P)$ is the real part of the admittance in the cell-attached configuration. The admittance of the sealed patch itself may be modeled as the series combination of patch capacitance C_P and series resistance R_A in parallel with the leak conductance G_L. The average charging time constant $\tau_{patch} = R_A C_P$ was found to be 2.4 μs. The real part of patch admittance may thus be written as

$$\mathrm{Re}(Y_P) = G_L + \frac{(2\pi f \tau_{patch})^2}{R_A[1 + (2\pi f \tau_{patch})^2]}.$$

This result indicates that a fast patch time constant is desirable for low noise. As typical values we assumed G_L = 100 pS, τ_{patch} = 2.4 μs, and R_A = 5 MΩ. The part charged with a time constant of 2.4 μs thus corresponds to a capacitance of ~0.5 pF and probably consists of the patch itself and some part of the pipette tip. The remaining fast pipette capacitance may thus be added in parallel to the admittance as a pure capacitor and should not contribute significantly to the real part. Measurements with smaller τ_{patch} will have lower noise. For the theoretical curve (Fig. 9, *red line*) we thus used our lowest value, τ_{patch} = 1.4 μs, and the standard values G_L = 100 pS, R_A = 5 MΩ. The sum of all of the contributions is shown as the black line in Fig. 9. It should be noted that in the frequency range of 0.8–80 kHz the noise contributed from the patch admittance and the amplifier noise are the most important contributions. The increase in e_n-C_t noise is negligible. With these assumptions the expected noise is very close to the data points of our best patch (Fig. 7).

We thank Irene Wunderlich and Regina Hinz-Herkommer for excellent technical assistance.

This work has been supported by the Deutsche Forschungsgemeinschaft (LI443/9-2 and Human Frontiers Science Programme grant R60227).

REFERENCES

Albillos, A., G. Dernick, H. Horstmann, W. Almers, G. Alvarez de Toledo, and M. Lindau. 1997. The exocytotic event in chromaffin cells revealed by patch amperometry. *Nature.* 389:509–512.

Alés, E., L. Tabares, J. M. Poyato, V. Valero, M. Lindau, and G. Alvarez de Toledo. 1999. High calcium concentrations shift the mode of exocytosis to the kiss-and-run mechanism. *Nature Cell Biol.* 1:40–44.

Alvarez de Toledo, G., and J. M. Fernandez. 1987. The events leading to secretory granule fusion. *In* Cell Physiology of Blood. The Rockefeller University Press, New York. 332–344.

Alvarez de Toledo, G., R. Fernández-Chacón, and J. M. Fernandez. 1993. Release of secretory products during transient vesicle fusion. *Nature.* 363:554–558.

Barnett, D. W., and S. Misler. 1997. An optimized approach to membrane capacitance estimation using dual-frequency excitation. *Biophys. J.* 72: 1641–1658.

Benndorf, K. 1995. Low-noise recording. *In* Single-Channel Recording. Plenum Press, New York. 129–145.

Breckenridge, L. J., and W. Almers. 1987. Currents through the fusion pore that forms during exocytosis of a secretory vesicle. *Nature.* 328: 814–817.

Curran, M. J., F. S. Cohen, D. E. Chandlers, P. J. Munson, and J. Zimmerberg. 1993. Exocytotic fusion pores exhibit semi-stable states. *J. Membr. Biol.* 133:61–75.

Debus, K., J. Hartmann, G. Kilic, and M. Lindau. 1995. Influence of conductance changes on patch clamp capacitance measurements using a lock-in amplifier and limitations of the phase tracking technique. *Biophys. J.* 69:2808–2822.

Donelly, D. F. 1994. A novel method for rapid measurement of membrane resistance, capacitance, and access resistance. *Biophys. J.* 66:873–877.

Fernandez, J. M., E. Neher, and B. D. Gomperts. 1984. Capacitance measurements reveal stepwise fusion events in degranulating mast cells. *Nature.* 312:453–455.

Fidler, N., and J. M. Fernandez. 1989. Phase tracking: an improved phase detection technique for cell membrane capacitance measurements. *Biophys. J.* 56:1153–1162.

Gillis, K. D. 1995. Techniques for membrane capacitance measurements. *In* Single-Channel Recording, 2nd Ed. Plenum Press, New York. 155–198.

Hamill, O. P., A. Marty, E. Neher, B. Sakmann, and F. J. Sigworth. 1981. Improved patch-clamp technique for high-resolution current recording from cells and cell-free membrane patches. *Pflügers Arch. Eur. J. Physiol.* 391:85–100.

Hartmann, J., and M. Lindau. 1995. A novel Ca^{2+}-dependent step in exocytosis subsequent to vesicle fusion. *FEBS Lett.* 363:217–220.

Hartmann, J., S. Scepek, and M. Lindau. 1995. Regulation of granule size in human and horse eosinophils by number of fusion events among unit granules. *J. Physiol. (Lond.).* 483:201–209.

Joshi, C., and J. M. Fernandez. 1988. Capacitance measurements: an analysis of the phase detector technique used to study exocytosis and endocytosis. *Biophys. J.* 53:885–892.

Kreft, M., and R. Zorec. 1997. Cell-attached measurements of attofarad capacitance steps in rat melanotrophs. *Pflügers Arch. Eur. J. Physiol.* 434:212–214.

Levis, R. A., and J. L. Rae. 1993. The use of quartz pipettes for low noise single channel recording. *Biophys. J.* 65:1666–1677.

Levis, R. A., and J. L. Rae. 1998. Low-noise patch-clamp techniques. *Methods Enzymol.* 293:218–266.

Lindau, M. 1991. Time-resolved capacitance measurements: monitoring exocytosis in single cells. *Q. Rev. Biophys.* 24:75–101.

Lindau, M. 1998. Fusion proteins and the fusion events. *In* Toxins and the Secretory System. Harwood Academic Publishers, Reading, UK. 131–146.

Lindau, M., and W. Almers. 1995. Structure and function of fusion pores in exocytosis and ectoplasmic membrane fusion. *Curr. Opin. Cell Biol.* 7:509–517.

Lindau, M., and E. Neher. 1988. Patch-clamp techniques for time-resolved capacitance measurements in single cells. *Pflügers Arch. Eur. J. Physiol.* 411:137–146.

Lindau, M., O. Nüsse, J. Bennett, and O. Cromwell. 1993. The membrane fusion events in degranulating guinea pig eosinophils. *J. Cell Sci.* 104:203–209.

Lollike, K., N. Borregaard, and M. Lindau. 1995. The exocytotic fusion pore of small granules has a conductance similar to an ion channel. *J. Cell Biol.* 129:99–104.

Lollike, K., N. Borregaard, and M. Lindau. 1998. Capacitance flickers and "pseudoflickers" of small granules, measured in the cell attached configuration. *Biophys. J.* 75:53–59.

Morgan, A., and R. D. Burgoyne. 1997. Common mechanisms for regulated exocytosis in the chromaffin cell and the synapse. *Semin. Cell Dev. Biol.* 8:141–149.

Neher, E., and A. Marty. 1982. Discrete changes of cell membrane capacitance observed under conditions of enhanced secretion in bovine adrenal chromaffin cells. *Proc. Natl. Acad. Sci. USA.* 79:6712–6716.

Nührmann, D. 1994. Das grosse Werkbuch Elektronik. Franzis-Verlag, Poing.

Oberhauser, A. F., and J. M. Fernandez. 1996. A fusion pore phenotype in mast cells of the ruby-eye mouse. *Proc. Natl. Acad. Sci. USA.* 93: 14349–14354.

Oberhauser, A. F., J. R. Monck, and J. M. Fernandez. 1992. Events leading to the opening and closing of the exocytotic fusion pore have markedly different temperature dependencies. *Biophys. J.* 61:800–809.

Ratinov, V., I. Plonsky, and J. Zimmerberg. 1998. Fusion pore conductance: experimental approaches and theoretical algorithms. *Biophys. J.* 74:2374–2387.

Robinson, I. M., J. M. Finnegan, J. R. Monck, R. M. Wightman, and J. M. Fernandez. 1995. Colocalization of calcium-entry and exocytotic release sites in adrenal chromaffin cells. *Proc. Natl. Acad. Sci. USA.* 92: 2474–2478.

Rohlicek, V., and J. Rohlicek. 1993. Measurement of membrane capacitance and resistance of single cells with two frequencies. *Physiol. Res.* 42:423–428.

Rohlicek, V., and A. Schmid. 1994. Dual-frequency method for synchronous measurement of cell capacitance, membrane conductance and access-resistance on single cells. *Pflügers Arch. Eur. J. Physiol.* 428: 30–38.

Sakmann, B., and E. Neher. 1983. Geometric parameters of pipettes and membrane patches. *In* Single Channel Recording. Plenum Press, New York. 37–51.

Sigworth, F. J. 1995. Electronic design of the patch clamp. *In* Single Channel Recording. Plenum Press, New York. 95–125.

Sine, S. M., T. Claudio, and F. J. Sigworth. 1990. Activation of *Torpedo* acetylcholine receptors expressed in mouse fibroblasts. Single channel current kinetics reveal distinct agonist binding affinities. *J. Gen. Physiol.* 96:395–437.

Söllner, T., S. Whiteheart, M. Brunner, H. Erdjument-Bromage, M. Geromanos, P. Tempst, and J. E. Rothman. 1993. SNAP receptors implicated in vesicle targeting and fusion. *Nature.* 362:318–323.

Spruce, A. E., L. J. Breckenridge, A. K. Lee, and W. Almers. 1990. Properties of the fusion pore that forms during exocytosis of a mast cell secretory vesicle. *Neuron.* 4:643–654.